



Deposited via The University of Sheffield.

White Rose Research Online URL for this paper:

<https://eprints.whiterose.ac.uk/id/eprint/187180/>

Version: Published Version

---

**Article:**

Feng, P., Xu, C., Bai, J. et al. (2022) A simple approach to achieving ultrasmall III-nitride microlight-emitting diodes with red emission. *ACS Applied Electronic Materials*, 4 (6). pp. 2581-3165. ISSN: 2637-6113

<https://doi.org/10.1021/acsaelm.2c00311>

---

**Reuse**

This article is distributed under the terms of the Creative Commons Attribution (CC BY) licence. This licence allows you to distribute, remix, tweak, and build upon the work, even commercially, as long as you credit the authors for the original work. More information and the full terms of the licence here:

<https://creativecommons.org/licenses/>

**Takedown**

If you consider content in White Rose Research Online to be in breach of UK law, please notify us by emailing [eprints@whiterose.ac.uk](mailto:eprints@whiterose.ac.uk) including the URL of the record and the reason for the withdrawal request.

# A Simple Approach to Achieving Ultrasmall III-Nitride Microlight-Emitting Diodes with Red Emission

Peng Feng,<sup>+</sup> Ce Xu,<sup>+</sup> Jie Bai,<sup>+</sup> Chenqi Zhu, Ian Farrer, Guillem Martinez de Arriba, and Tao Wang\*

Cite This: <https://doi.org/10.1021/acsaelm.2c00311>

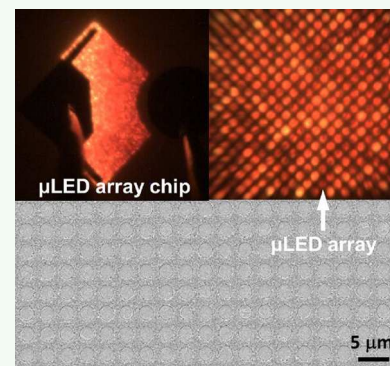
Read Online

ACCESS |

Metrics & More

Article Recommendations

**ABSTRACT:** The microdisplays for augmented reality and visual reality require ultrasmall microlight-emitting diodes ( $\mu$ LEDs) with a dimension of  $\leq 5 \mu\text{m}$ . Furthermore, the microdisplays also need three kinds of such  $\mu$ LEDs each emitting red, green, and blue emission. Currently, in addition to a great challenge for achieving ultrasmall  $\mu$ LEDs mainly based on III-nitride semiconductors, another fundamental barrier is due to extreme difficulty in growing III-nitride-based red LEDs. So far, there has not been any effective approach to obtain high indium content InGaN as an active region required for a red LED while maintaining high optical performance. In this paper, we have demonstrated a selective epitaxy growth approach on a template featuring microhole arrays. This allows us to not only obtain the natural formation of ultrasmall  $\mu$ LEDs but also achieve InGaN with enhanced indium content at an elevated growth temperature, at which it is impossible to obtain InGaN-based red LEDs on a standard planar surface. By means of this approach, we have demonstrated red  $\mu$ LEDs (at an emission wavelength of 642 nm) with a dimension of  $2 \mu\text{m}$ , exhibiting a high luminance of  $3.5 \times 10^7 \text{ cd/m}^2$  and a peak external quantum efficiency of 1.75% measured in a wafer form (i.e., without any packaging to enhance an extraction efficiency). In contrast, an LED grown under identical growth conditions but on a standard planar surface shows green emission at 538 nm. This highlights that our approach provides a simple solution that can address the two major challenges mentioned above.



**KEYWORDS:** InGaN, microLED, selective epitaxy growth, patterned template, MOVPE, EQE

## 1. INTRODUCTION

There is a growing interest for developing microdisplays with compact screens of  $\leq 1/4$ " diagonal length, which have a wide range of applications in smart watches, smart phones, smart bands, and augmented reality and virtual reality (AR & VR) devices.<sup>1–5</sup> Their individual pixel elements typically consist of a large number of microscale visible LEDs mainly based on III-nitride semiconductors, which are referred to as microLEDs ( $\mu$ LEDs). For instance, the microdisplays for AR and VR require  $\mu$ LEDs with an ultrasmall dimension of  $\leq 5 \mu\text{m}$ .<sup>6–8</sup> Such devices are typically utilized in a scenario where spaces are small or the devices need to be close to the eyes. Therefore, the devices require high resolution, high contrast ratio, high luminance, and high external quantum efficiency (EQE).<sup>9,10</sup> Of course, a microdisplay needs three kinds of individual  $\mu$ LEDs as a single pixel each emitting red, green, and blue emission (i.e., RGB), respectively.

InGaN semiconductors have direct bandgaps across their whole content ranging from 0.7 eV for InN to 3.43 eV for GaN, covering part of the infrared region, the full visible spectrum, and part of the ultraviolet (UV) region. So far, InGaN-based  $\mu$ LEDs with reasonably good performance in the blue and green spectral region have been reported. However, red LEDs still rely on AlGaInP materials. Although a large area

AlGaInP red LED with a high efficiency of  $>50\%$  can be obtained,<sup>11</sup> the efficiency reduces dramatically when its dimension is reduced to the microscale, namely,  $\mu$ LEDs. This is due to an enhancement in the surface recombination rate and the long diffusion lengths of carriers.<sup>12–15</sup> Moreover, the efficiency of AlGaInP red LEDs is sensitive to their junction temperature,<sup>16,17</sup> and thus, AlGaInP red LEDs generally suffer from a severe leakage current at a high temperature, generating a severe efficiency thermal drop. All these fundamental issues indicate that it is indispensable to develop III-nitride-based red LEDs to meet the requirements for the fabrication of a full color microdisplay.

InGaN with high indium content ( $>20\%$ ) is necessary for obtaining long wavelength emission. Unfortunately, it is greatly challenging to achieve high indium content InGaN while maintaining high optical performance.<sup>18,19</sup> A typical method to achieve high indium content in InGaN is to lower the growth

Received: March 9, 2022

Accepted: May 10, 2022

62 temperature for InGaN. However, it is clear that this method is  
63 not ideal because it causes a significant degradation in crystal  
64 quality.

65 In general, vapor–solid thermodynamic equilibrium can be  
66 modified by stress, making the solid-phase epitaxial composi-  
67 tion reduce toward lattice-matched conditions. This is the  
68 major reason why it is difficult to increase indium  
69 incorporation into GaN.<sup>20–24</sup> Therefore, the growth of  
70 InGaN on a relaxed layer is beneficial for obtaining high  
71 indium content in InGaN. However, bear in mind that the  
72 formation of a relaxed layer is often associated with the  
73 generation of extra defects if a heterostructure with a large  
74 lattice mismatch is used to generate a relaxed layer. This leads  
75 to degradation in optical performance. Furthermore, the stress  
76 status of an underlying layer plays a critical role in determining  
77 indium incorporation into GaN. Generally speaking, tensile  
78 stress tends to enhance indium incorporation into GaN,  
79 offering a unique advantage for growing red LEDs on silicon  
80 substrates as GaN on Si suffering tensile stress.<sup>25,26</sup> In contrast,  
81 GaN grown on sapphire substrates exhibits compressive strain.

82 The growth of InGaN-based red LEDs has been reported by  
83 means of inserting a thin AlN or an AlGaIn layer into each  
84 InGaIn quantum well as an emitting region, leading to an  
85 enhancement in strain that pushes the emission wavelength of  
86 InGaIn quantum wells toward longer wavelength.<sup>27,28</sup> So far,  
87 this approach has become a popular method for the growth of  
88 long wavelength emitters, in particular, red LEDs.<sup>25–30</sup>  
89 Furthermore, by combining the idea of inserting a thin AlN  
90 or AlGaIn and further adjusting the in-plane strain of a GaN  
91 template by tuning the GaN thickness, 633 nm-wavelength red  
92 LEDs with an external quantum efficiency (EQE) of 1.6% has  
93 been reported, where an extremely thick GaN (8–10  $\mu\text{m}$ )  
94 template has been employed.<sup>26,29</sup> A more recent work has  
95 demonstrated that a peak EQE as high as 4.5% has been  
96 achieved on red InGaIn  $\mu\text{LEDs}$ .<sup>31</sup> However, it is worth noting  
97 that the approach of strain enhancing also leads to a reduction  
98 in internal quantum efficiency.

99 We expect that an enhanced relaxation can be achieved by  
100 using a selective epitaxy growth approach on a microhole-  
101 patterned template, which we have developed recently, where  
102  $\mu\text{LEDs}$  can be naturally formed but without employing any  
103 dry-etching techniques because selective epitaxy growth can  
104 take place only within these microholes.<sup>7,8</sup> In this work, we are  
105 proposing to employ this approach to achieve ultrasmall red  
106  $\mu\text{LED}$  arrays with enhanced quantum efficiency but without  
107 inserting any thin AlN or AlGaIn into InGaIn quantum wells as  
108 an emitting region. It is expected that no lateral confinement  
109 during the selective epitaxy growth process leads to strain  
110 relaxation effectively and naturally. By this mechanism, 642 nm  
111 red  $\mu\text{LEDs}$  with a dimension of 2  $\mu\text{m}$  have been achieved by  
112 our selective epitaxy growth conducted at an elevated  
113 temperature, at which a red LED cannot be achieved on a  
114 standard planar GaN surface. The resultant external quantum  
115 efficiency is 1.75%. For comparison, only 538 nm green LEDs  
116 on a standard planar GaN template can be obtained even  
117 under identical growth conditions. Our X-ray diffraction  
118 measurements have confirmed that a significant enhancement  
119 in indium content in InGaIn has been achieved by our  
120 approach.

## 2. RESULTS AND DISCUSSION

121 In this work, two different InGaIn-based LED samples have  
122 been designed and then grown, aiming to study the influence

of selective epitaxial growth on the optical performance of III-  
nitride LEDs grown on a prepatterned template featuring  
microhole arrays. A  $\mu\text{LED}$  array sample is obtained by our  
selective epitaxy growth on the prepatterned n-GaN template  
as mentioned above and is denoted as LED A. The other one is  
a normal LED sample grown under identical growth but on a  
standard planar n-GaN template without any features and is  
denoted as LED B.

Silicon-doped n-GaN epiwafers are first grown on *c*-plane  
(0001) sapphire substrates using the standard two-step  
approach by a metalorganic vapor phase epitaxy (MOVPE)  
technique. Initially, a 25 nm GaN nucleation layer is prepared  
at a low temperature after the substrate is subject to a  
thermally annealing process at a high temperature of 1150  $^{\circ}\text{C}$ ,  
followed by a 1  $\mu\text{m}$  GaN buffer layer, and then another 500 nm  
silicon-doped n-GaN layer both grown at a high temperature of  
1120  $^{\circ}\text{C}$ . For LED A, the n-GaN template is further patterned  
into microhole arrays using SiO<sub>2</sub> masks on its top, which is  
then used as a prepatterned template for our selective epitaxial  
growth.

Figure 1a shows the schematics of our selective epitaxy  
growth approach, allowing us to naturally achieve  $\mu\text{LED}$  arrays

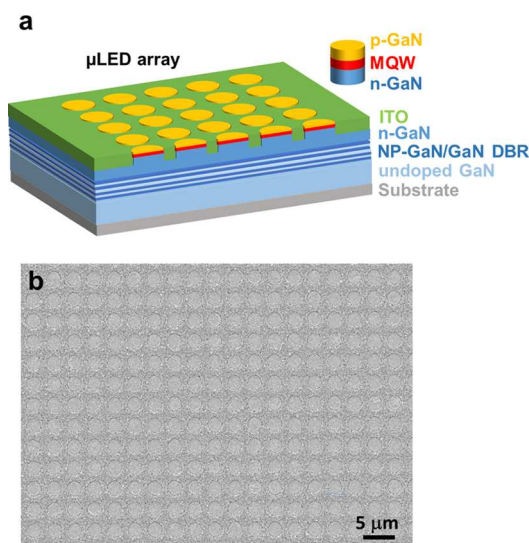


Figure 1. (a) Schematic of selective epitaxy growth and (b) plan-view SEM image for the  $\mu\text{LED}$  array epiwafer, showing a diameter of 2  $\mu\text{m}$  and an interpitch of 1.5  $\mu\text{m}$ .

without involving any dry-etching process, i.e., LED A. For the  
detailed information on fabricating the prepatterned templates,  
refer to the [Experimental Methods](#) section.

Afterward, a standard III-nitride LED structure is selectively  
grown on the micropatterned template by MOVPE, namely, a  
silicon-doped n-GaN layer is first prepared, followed by an  
In<sub>0.05</sub>Ga<sub>0.95</sub>N/GaN superlattice (SLS) structure as a prelayer,  
five periods of InGaIn/GaN multiple quantum wells (MQWs)  
as an emitting region, then a 20 nm *p*-type Al<sub>0.2</sub>Ga<sub>0.8</sub>N as an  
electron blocking layer, and a final 150 nm *p*-type GaN layer.  
The total thickness of the overgrown layers is 500 nm, which  
matches the thickness of the SiO<sub>2</sub> masks. Due to the SiO<sub>2</sub>  
masks, the growth of the LED structure takes place within the  
microholes only, naturally forming regularly arrayed  $\mu\text{LEDs}$ .

A Raith 150 scanning electron microscopy (SEM) system  
has been used to characterize the surface morphology of our  
regularly arrayed  $\mu\text{LEDs}$ . Figure 1b shows a typical plan-view

162 SEM image of our regularly arrayed  $\mu$ LEDs wafer (i.e., LED  
163 A), exhibiting a nice circular shape with an excellent high  
164 uniformity in shape, diameter, and interpitch. All  $\mu$ LEDs are 2  
165  $\mu\text{m}$  in diameter and only 1.5  $\mu\text{m}$  in interpitch. Such a small  
166 diameter and an interpitch are crucial for manufacturing a  
167 high-resolution microdisplay in a compact manner. Further-  
168 more, the  $\mu$ LED pixels share a common  $n$  contact while all the  
169  $p$  contacts are left open. As a result, our regularly arrayed  
170  $\mu$ LED epiwafers well match any existing manufacturing  
171 technique of microdisplays, for instance, the pick-and-place  
172 technology, which has been widely used,<sup>32</sup> and the integrating  
173 technique using driving transistors based on the silicon CMOS  
174 IC to achieve individually addressable  $\mu$ LED-based microdis-  
175 plays.<sup>33</sup>

176 A high-resolution X-ray diffractometer (HRXRD) (Bruker  
177 D8) has been employed to determine the indium content of  
178 the InGaN MQWs by performing  $\omega$ - $2\theta$  scan measurements  
179 along the (002) direction, together with a fitting using the  
180 Bruker JV-RADS simulation software. Figure 2a,b shows the

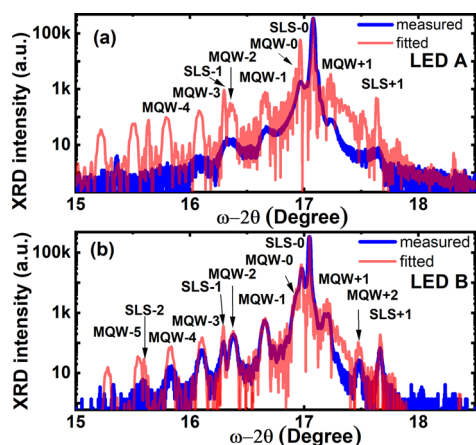


**Figure 2.** HRXRD  $\omega$ - $2\theta$  scan curves of the  $\mu$ LED array sample on a patterned template, i.e., (a) LED A, and the LED sample grown on a standard planar template, i.e., (b) LED B under identical conditions. Fittings have also been provided to determine the indium content in InGaN MQWs.

181 HRXRD  $\omega$ - $2\theta$  scan curves of our regularly arrayed  $\mu$ LED wafer  
182 (i.e., LED A) and the standard LED wafer (i.e., LED B),  
183 respectively. In both cases, the satellite peaks with up to 4 or 5  
184 orders from the InGaN/GaN MQWs have been clearly  
185 observed. The satellite peaks from the SLS structure as a  
186 prelayer have also been observed. Based on a detailed fitting, it  
187 can be determined that the indium content of the InGaN  
188 MQWs of LED A is 31% and that the thicknesses of the  
189 InGaN quantum well and the barrier are 2.2 and 13.8 nm,  
190 respectively. In contrast, LED B exhibits 24% indium content  
191 in the InGaN MQWs with a 2.6 nm quantum well and a 14.1  
192 nm barrier. The XRD fittings are conducted based on fully  
193 strained InGaN MQWs for both LEDs. It is well known that  
194 strain relaxation will reduce the strain-induced quantum-  
195 confined Stark effect (QCSE), leading to a blue-shift in the  
196 emission. It means that if the InGaN MQWs are assumed to be  
197 strain-relaxed, the indium content should be even higher. In  
198 consideration of a higher chance of strain relaxation for the  
199  $\mu$ LEDs, the fitted values of indium contents represent the least  
200 difference between the two LEDs. This direct comparison  
201 indicates that enhanced indium content in InGaN MQWs can

be obtained by using our selective epitaxy growth approach on 202  
a prepatterned template featuring microhole arrays. 203

Finally, both the regularly arrayed  $\mu$ LED wafer (i.e., LED A) 204  
and the standard LED wafer (i.e., LED B) have been fabricated 205  
into LED devices with an area of  $330 \times 330 \mu\text{m}^2$ . For the 206  
detailed information about device fabrication, refer to the 207  
**Experimental Methods** section. For LED A, each LED device 208  
consists of a few thousands of 2  $\mu\text{m}$   $\mu$ LEDs connected. In this 209  
work, the  $\mu$ LEDs in LED A share a common  $p$  contact and  $n$  210  
contact, which are driven simultaneously in all electro- 211  
luminescence (EL) measurements. However, it is worth noting 212  
that our arrayed  $\mu$ LEDs are designed to make the  $p$  contacts of 213  
each  $\mu$ LED left open, providing an opportunity in the future to 214  
allow indium bumps to be bonded to an active matrix driving 215  
transistors. This means that our regularly arrayed  $\mu$ LED 216  
structure entirely matches any existing individually addressable 217  
 $\mu$ LED microdisplays. 218

For a direct comparison, the LED B wafer has also been 219  
processed under identical conditions in the same batch. All the 220  
characteristics of our  $\mu$ LED chips in the present study have 221  
been carried out on bare chips, meaning that we did not use 222  
coating or passivation or epoxy or reflector for improving 223  
extraction efficiency. Current–voltage ( $I$ - $V$ ) characteristic and 224  
EL measurements have been performed at room temperature 225  
in continuous wave (CW) mode using a Keithley 2400 226  
sourcemeater on a probe station equipped with an optical 227  
microscopy system. 228

The EL spectra have been measured on the two LED devices 229  
under identical conditions aiming to make a direct comparison. 230  
For instance, Figure 3a,b shows the EL spectra of the two LED 231  
devices measured at a current density of 10  $\text{A}/\text{cm}^2$ , 232  
respectively. Both spectra exhibit a single emission peak. The 233

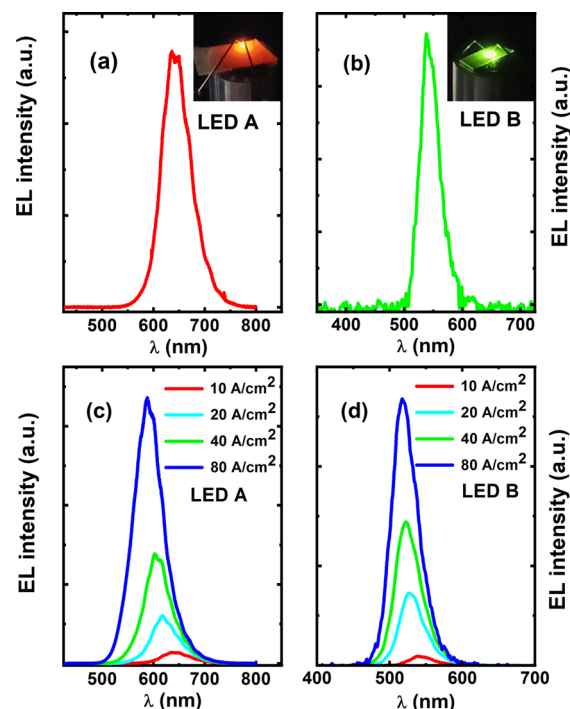


**Figure 3.** EL spectra measured at 10  $\text{A}/\text{cm}^2$  for the  $\mu$ LED array device, i.e., (a) LED A and (b) LED B, where the insets show their respective emission images. EL spectra measured at increased current densities from 10 to 80  $\text{A}/\text{cm}^2$  for (c) LED A and (d) LED B, respectively.

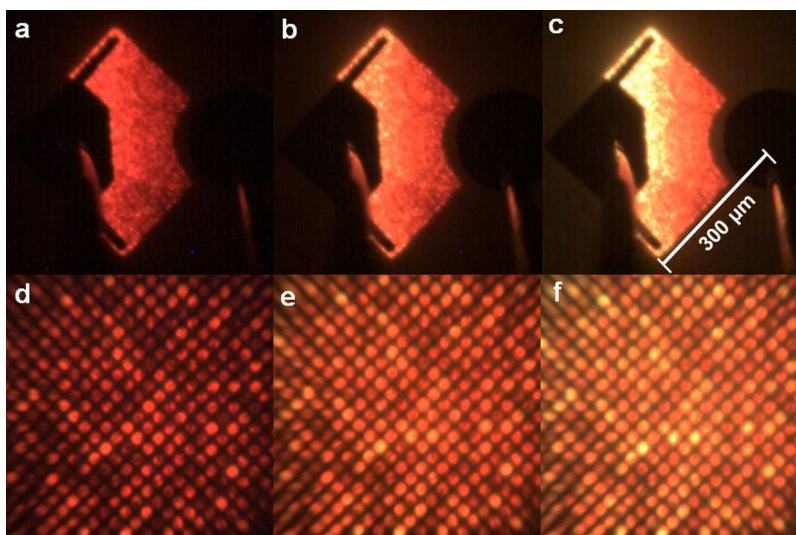


**Figure 4.** Emission images of the  $\mu$ LED array device taken using an optical microscopy system as a function of injection current density (4, 8, and 12  $\text{A}/\text{cm}^2$ ) under (a–c) a low magnification and (d–f) a high magnification, respectively.

234  $\mu$ LED array device shows a strong emission at an emission  
 235 wavelength of 642 nm in the red spectral region. The inset of  
 236 Figure 3a exhibits an emission image of the  $\mu$ LED array chip,  
 237 demonstrating red light. In contrast, Figure 3b displays a  
 238 strong green emission at 538 nm from the LED B device also  
 239 measured at 10  $\text{A}/\text{cm}^2$ , and the inset displays its emission  
 240 image. This means that the selective epitaxial growth on a  
 241 prepatterned template featuring regularly arrayed microholes  
 242 results in a red-shift of about 100 nm in emission wavelength in  
 243 comparison with the LED grown on a standard planar GaN  
 244 surface, although both are grown under identical growth  
 245 conditions. As discussed earlier, the growth of InGaN on a  
 246 relaxed layer is beneficial for obtaining high indium content in  
 247 InGaN. Due to no lateral confinement during the overgrowth  
 248 within the microholes, the overgrown n-GaN is very likely  
 249 strain-relaxed, which leads to an enhancement in the indium  
 250 content in the overlying InGaN MQWs. Combined with the  
 251 XRD results, it has been confirmed that our selective epitaxy  
 252 growth approach can enhance indium incorporation into GaN  
 253 significantly. Figure 3c,d shows the EL spectra of LED A and  
 254 LED B, both measured as a function of injection current  
 255 density ranging from 10 to 80  $\text{A}/\text{cm}^2$ , respectively.

256 In order to demonstrate emitting  $\mu$ LED pixels, optical  
 257 microscopy images have been taken using a micro-EL  
 258 measurement system where emissions are collected through  
 259 two objective lenses (one 10 $\times$  magnification lens with NA =  
 260 0.28 and another 50 $\times$  magnification lens with NA = 0.43).  
 261 Figure 4a–c displays the emission images of our  $\mu$ LED array  
 262 chip taken under 4, 8, and 12  $\text{A}/\text{cm}^2$  current density,  
 263 respectively, while Figure 4d–f provides their corresponding  
 264 emission images taken under a high magnification, showing  
 265 strong red emissions from individual 2  $\mu\text{m}$   $\mu$ LED pixels even  
 266 under low current densities. It is worth mentioning that such  
 267 low current densities used for the operation of our  $\mu$ LEDs are  
 268 lower than a typical current density (22  $\text{A}/\text{cm}^2$ ) for the  
 269 operation of a conventional broad area LED.

270 Both light output powers and luminous flux have been  
 271 measured on the bare-chip LEDs bonded on TOS-headers in  
 272 CW mode using a LCS-100 integrating sphere equipped with a  
 273 CCD APRAR spectrometer. Figure 5a–c shows the output  
 274 power, luminance, and EQE of the  $\mu$ LED array device (i.e.,

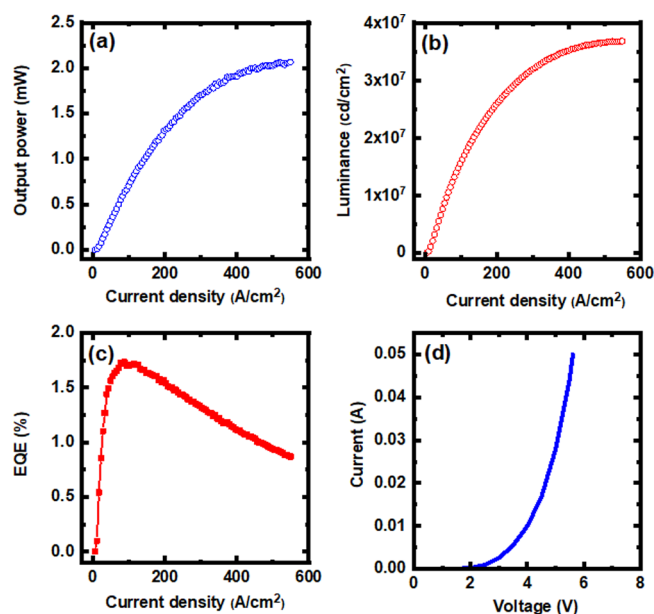


**Figure 5.** (a) Output power, (b) luminance, (c) EQE, and (d) current–voltage characteristics of the  $\mu$ LED array device (i.e., LED A).

275 LED A) as a function of injection current density. This  
 276 demonstrates that the output power and luminescence increase  
 277 monolithically with increasing current density up to 450  $\text{A}/\text{cm}^2$   
 278 and that a high luminance of  $3.5 \times 10^7$   $\text{cd}/\text{m}^2$  has been  
 279 achieved. The peak EQE is about 1.75%. It is worth  
 280 highlighting that although there are not any heat-sink  
 281 components used, our ultrasmall  $\mu$ LEDs can still sustain a  
 282 high current density of above 450  $\text{A}/\text{cm}^2$ , also confirming the  
 283 high crystal quality of our  $\mu$ LED array sample achieved by our  
 284 selective epitaxy growth approach. Figure 5d displays the  
 285 typical  $I$ – $V$  characteristics of LED A measured as a function of  
 286 bias, which is similar to that of the LED B device. This also  
 287 shows the good electrical property of our  $\mu$ LED array device.

### 3. CONCLUSIONS

288 In summary, we are proposing to employ a selective epitaxy  
289 growth approach on a microhole patterned template to  
290 significantly enhance strain relaxation, allowing us to not  
291 only obtain the natural formation of regularly arrayed  $\mu$ LEDs  
292 but also achieve enhanced indium content in the InGaN/GaN  
293 MQWs used as an active region for the  $\mu$ LEDs. By means of  
294 this approach, we have demonstrated red InGaN-based  $\mu$ LED  
295 arrays with a dimension of  $2\ \mu\text{m}$  and an interpitch of  $1.5\ \mu\text{m}$ . A  
296 high luminance of  $3.5 \times 10^7\ \text{cd/m}^2$  and a peak EQE of 1.7%  
297 have been achieved for the red  $\mu$ LED array chip in a wafer  
298 form without any packaging. In contrast, the standard LED  
299 grown under growth conditions but on a standard planar GaN  
300 template demonstrates green emission. This means that our  
301 approach paves the way for achieving long wavelength InGaN-  
302 based  $\mu$ LEDs with ultrasmall dimensions at an elevated growth  
303 temperature, at which it is impossible to obtain InGaN-based  
304 red LEDs on a standard planar template.

### 4. EXPERIMENTAL METHODS

305 **4.1. Fabrication of Prepatterned Templates.** A 500 nm  $\text{SiO}_2$   
306 dielectric film is deposited on the n-GaN template by a plasma-  
307 enhanced chemical vapor deposition (PECVD) technique, followed  
308 by employing a standard photolithography and then a dry etching  
309 technique to selectively etch the  $\text{SiO}_2$  dielectric layer down to the n-  
310 GaN surface by inductively coupled plasma (ICP), forming regularly  
311 arrayed microholes with a diameter of  $2\ \mu\text{m}$  and an interpitch of  $1.5$   
312  $\mu\text{m}$ . This prepatterned template will then be used for further selective  
313 epitaxy growth. Finally,  $\mu$ LEDs will be selectively grown only within  
314  $\text{SiO}_2$  microhole regions, naturally forming regularly arrayed  $\mu$ LEDs.

315 **4.2. Device Fabrication.** Indium-tin-oxide (ITO) is deposited  
316 and then undergoes an annealing process in air at  $600\ ^\circ\text{C}$  for 1 min,  
317 forming transparent *p*-type contact, while Ti/Al/Ni/Au alloys are  
318 prepared as *n*-type contact. Ti/Au alloys are used as *p*-type and *n*-type  
319 electrodes. All the characteristics of the LEDs in this paper are  
320 conducted on bare chips, namely, no coating, no passivation, no  
321 epoxy, or no reflector, which are often employed for obtaining  
322 enhanced extraction efficiency.

### ■ AUTHOR INFORMATION

#### Corresponding Author

325 **Tao Wang** – Department of Electronic and Electrical  
326 Engineering, The University of Sheffield, Sheffield S1 3JD,  
327 United Kingdom; [orcid.org/0000-0001-5976-4994](https://orcid.org/0000-0001-5976-4994);  
328 Email: [t.wang@sheffield.ac.uk](mailto:t.wang@sheffield.ac.uk)

#### Authors

330 **Peng Feng** – Department of Electronic and Electrical  
331 Engineering, The University of Sheffield, Sheffield S1 3JD,  
332 United Kingdom  
333 **Ce Xu** – Department of Electronic and Electrical Engineering,  
334 The University of Sheffield, Sheffield S1 3JD, United Kingdom  
335 **Jie Bai** – Department of Electronic and Electrical Engineering,  
336 The University of Sheffield, Sheffield S1 3JD, United Kingdom  
337 **Chenqi Zhu** – Department of Electronic and Electrical  
338 Engineering, The University of Sheffield, Sheffield S1 3JD,  
339 United Kingdom  
340 **Ian Farrer** – Department of Electronic and Electrical  
341 Engineering, The University of Sheffield, Sheffield S1 3JD,  
342 United Kingdom  
343 **Guillem Martinez de Arriba** – Department of Electronic and  
344 Electrical Engineering, The University of Sheffield, Sheffield  
345 S1 3JD, United Kingdom

346 Complete contact information is available at:

<https://pubs.acs.org/10.1021/acsaelm.2c00311>

347

### Author Contributions

<sup>†</sup>P.F., C.X., and J.B. contributed equally to this work.

### Author Contributions

T.W. conceived the idea and organized the project. T.W. and J.B. prepared the manuscript. P.F., X.C., and C.Z. grew all the samples. P.F., X.C., and I.F. performed the material characterization. J.B. and G.M.D.A. fabricated the prepatterned templates and carried out the device fabrication. J.B. conducted the device characterization.

### Notes

The authors declare no competing financial interest.

### ■ ACKNOWLEDGMENTS

Financial support from the Engineering and Physical Sciences Research Council (EPSRC), UK via EP/P006973/1, EP/M015181/1, and EP/P006361/1 is acknowledged.

### ■ REFERENCES

- (1) Meng, W.; Xu, F.; Yu, Z.; Tao, T.; Shao, L.; Liu, L.; Li, T.; Wen, K.; Wang, J.; He, L.; Sun, L.; Li, W.; Ning, H.; Dai, N.; Qin, F.; Tu, X.; Pan, D.; He, S.; Li, D.; Zheng, Y.; Lu, Y.; Liu, B.; Zhang, R.; Shi, Y.; Wang, X. Three-dimensional Monolithic Micro-LED Display Driven by Atomically Thin Transistor matrix. *Nat. Nanotechnol.* **2021**, *16*, 1231.
- (2) Park, J.; Choi, J. H.; Kong, K.; Han, J. H.; Park, J. H.; Kim, N.; Lee, E.; Kim, D.; Ki, J.; Chung, D.; Jun, S.; Kim, M.; Yoon, E.; Shin, J.; Hwang, S. Electrically Driven Mid-Submicrometre Pixelation of InGaN Micro-Light-Emitting Diode Displays for Augmented-Reality Glasses. *Nat. Photonics* **2021**, *15*, 449.
- (3) Huang, Y.; Hsiang, E.-L.; Deng, M.-Y.; Wu, S.-T. Mini-LED, Micro-LED and OLED Displays: Present Status and Future Perspectives. *Light: Sci. Appl.* **2020**, *9*, 105.
- (4) Han, H.-V.; Lin, H.-Y.; Lin, C.-C.; Chong, W.-C.; Li, J.-R.; Chen, K.-J.; Chen, T.-M.; Chen, H.-M.; Lau, K.-M.; Kuo, H.-C. Resonant-enhanced full-color Emission of Quantum-Dot-Based Micro LED Display Technology. *Opt. Express* **2015**, *23*, 32504–32515.
- (5) Green, R. P.; McKendry, J. J. D.; Massoubre, D.; Gu, E.; Dawson, M. D.; Kelly, A. E. Modulation Bandwidth Studies of recombination Processes in Blue and Green InGaN Quantum Well Micro-Light-Emitting Diodes. *Appl. Phys. Lett.* **2013**, *102*, No. 091103.
- (6) Ley, R. T.; Smith, J. M.; Wong, M. S.; Margalith, T.; Nakamura, S.; DenBaars, S. P.; Gordon, M. J. Revealing the Importance of Light Extraction Efficiency in InGaN/GaN MicroLEDs via Chemical Treatment and Dielectric Passivation. *Appl. Phys. Lett.* **2020**, *116*, 251104.
- (7) Bai, J.; Cai, Y.; Feng, P.; Fletcher, P.; Zhao, X.; Zhu, C.; Wang, T. A Direct Epitaxial Approach To Achieving Ultrasmall and Ultrabright InGaN Micro Light-Emitting Diodes ( $\mu$ LEDs). *ACS Photonics* **2020**, *7*, 411.
- (8) Bai, J.; Cai, Y.; Feng, P.; Fletcher, P.; Zhu, C.; Tian, Y.; Wang, T. Ultrasmall, Ultracompact and Ultrahigh Efficient InGaN Micro Light Emitting Diodes ( $\mu$ LEDs) with Narrow Spectral Line Width. *ACS Nano* **2020**, *14*, 6906.
- (9) Zhan, T.; Yin, K.; Xiong, J.; He, Z.; Wu, S.-T. Augmented Reality and Virtual Reality Displays: Perspectives and Challenges. *iScience* **2020**, *23*, No. 101397.
- (10) Liu, Z.; Lin, C.-H.; Hyun, B.-R.; Sher, C.-W.; Luo, B.; Lv, Z.; Jiang, F.; Wu, T.; Ho, C.-H.; Kuo, H.-C.; He, J.-H. Micro-light-emitting diodes with quantum dots in display technology. *Light: Sci. Appl.* **2020**, *9*, 83.
- (11) Krames, M. R.; Ochiai-Holcomb, M.; Höfler, G. E.; Carter-Coman, C.; Chen, E. I.; Tan, I. H.; Grillo, P.; Gardner, N. F.; Chui, H. C.; Huang, J. W.; Stockman, S. A.; Kish, F. A.; Craford, M. G.;

- 410 Tan, T. S.; Kocot, C. P.; Hueschen, M.; Posselt, J.; Loh, B.; Sasser, G.;  
411 Collins, D. High-Power Truncated-Inverted-Pyramid  
412  $(\text{Al}_x\text{Ga}_{1-x})_{0.5}\text{In}_{0.5}\text{P}/\text{GaP}$  Light-Emitting Diodes Exhibiting >50%  
413 External quantum efficiency. *Appl. Phys. Lett.* **1999**, *75*, 2365–2367.
- 414 (12) Boroditsky, M.; Gontijo, I.; Jackson, M.; Vrijen, R.;  
415 Yablonovitch, E.; Krauss, T.; Cheng, C. C.; Scherer, A.; Bhat, R.;  
416 Krames, M. Surface Recombination Measurements on III–V  
417 Candidate Materials for Nanostructure Light-Emitting Diodes. *J.*  
418 *Appl. Phys.* **2000**, *87*, 3497.
- 419 (13) Royo, P.; Stanley, R. P.; Ilegems, M.; Streubel, K.; Gulden, K.  
420 H. Experimental Determination of the Internal Quantum Efficiency of  
421 AlGaInP Microcavity Light-Emitting Diodes. *J. Appl. Phys.* **2002**, *91*,  
422 2563.
- 423 (14) Oh, J.-T.; Lee, S.-Y.; Moon, Y.-T.; Moon, J. H.; Park, S.; Hong,  
424 K. Y.; Song, K. Y.; Oh, C.; Shim, J.-I.; Jeong, H.-H.; Song, J.-O.;  
425 Amano, H.; Seong, T.-Y. Light Output Performance of Red AlGaInP-  
426 Based Light Emitting Diodes with Different Chip Geometries and  
427 Structures. *Opt. Express* **2018**, *26*, 11194.
- 428 (15) Wong, M. S.; Kearns, J. A.; Lee, C.; Smith, J. M.; Lynsky, C.;  
429 Lheureux, G.; Choi, H.; Kim, J.; Kim, C.; Nakamura, S.; Speck, J. S.;  
430 Denbaars, S. P. Improved Performance of AlGaInP Red Micro-Light-  
431 Emitting Diodes with Sidewall Treatments. *Opt. Express* **2020**, *28*,  
432 5787–5793.
- 433 (16) Yadav, A.; Titkov, I. E.; Sokolovskii, G. S.; Karpov, S. Y.;  
434 Dudelev, V. V.; Soboleva, K. K.; Strassburg, M.; Pietzonka, I.;  
435 Lugauer, H.-J.; Rafailo, E. U. Temperature Effects on Optical  
436 Properties and Efficiency of Red AlGaInP-Based Light Emitting  
437 Diodes under High Current Pulse Pumping. *J. Appl. Phys.* **2018**, *124*,  
438 No. 013103.
- 439 (17) Oh, C.-H.; Shim, J.-I.; Shin, D.-S. Current- and Temperature-  
440 Dependent Efficiency Droops in InGaN-Based Blue and AlGaInP-  
441 Based Red Light-Emitting Diodes. *Japanese. J. Appl. Phys.* **2019**, *58*,  
442 SCCC08.
- 443 (18) El-Masry, N. A.; Piner, E. L.; Liu, S. X.; Bedair, S. M. Phase  
444 Separation in InGaN Grown by Metalorganic Chemical Vapor  
445 Deposition. *Appl. Phys. Lett.* **1998**, *72*, 40.
- 446 (19) Wakahara, A.; Tokuda, T.; Dang, X.-Z.; Noda, S.; Sasaki, A.  
447 Compositional Inhomogeneity and Immiscibility of a GaInN Ternary  
448 Alloy. *Appl. Phys. Lett.* **1997**, *71*, 906–908.
- 449 (20) Inatomi, Y.; Kanagawa, Y.; Ito, T.; Suski, T. Theoretical Study  
450 of the Composition Pulling Effect in InGaN Metalorganic Vapor-  
451 Phase Epitaxy Growth. *Jpn. J. Appl. Phys.* **2017**, *56*, No. 078003.
- 452 (21) Wang, T. Topical Review: Development of Overgrown  
453 Semipolar GaN for High Efficiency Green/Yellow Emission. *Semi-*  
454 *cond. Sci. Technol.* **2016**, *31*, No. 093003.
- 455 (22) Pereira, S.; Correia, M. R.; Pereira, E.; O'Donnell, K. P.; Alves,  
456 E.; Sequeira, A. D.; Franco, N.; Watson, I. M.; Deatcher, C. J. Strain  
457 and Composition Distributions in Wurtzite InGaN/GaN Layers  
458 Extracted from X-ray Reciprocal Space Mapping. *Appl. Phys. Lett.*  
459 **2002**, *80*, 3913.
- 460 (23) Shimizu, M.; Kawaguchi, Y.; Hiramatsu, K.; Sawaki, N.  
461 Metalorganic Vapor Phase Epitaxy of Thick InGaN on Sapphire  
462 Substrate. *Jpn. J. Appl. Phys., Part 1* **1997**, *36*, 3381.
- 463 (24) Sonderegger, S.; Feltin, E.; Merano, M.; Crottini, A.; Carlin, J.  
464 F.; Sachot, R.; Deveaud, B.; Grandjean, N.; Ganière, J. D. High Spatial  
465 Resolution Picosecond Cathodoluminescence of InGaN Quantum  
466 Wells. *Appl. Phys. Lett.* **2006**, *89*, 232109.
- 467 (25) Tawfik, W. Z.; Hyun, G. Y.; Ryu, S.-W.; Ha, J. S.; Lee, J. K.  
468 Piezoelectric Field in Highly Stressed GaN-Based LED on Si (1 1 1)  
469 Substrate. *Opt. Mater.* **2016**, *55*, 17–21.
- 470 (26) Iida, D.; Zhuang, Z.; Kirilenko, P.; Velazquez-Rizo, M.; Najmi,  
471 M. A.; Ohkawaa, K. High-color-Rendering-Index Phosphor-Free  
472 InGaN-Based White Light-Emitting Diodes by Carrier Injection  
473 Enhancement via V-Pits. *Appl. Phys. Lett.* **2020**, *116*, 162101.
- 474 (27) Hwang, J.-I.; Hashimoto, R.; Saito, S.; Nunoue, S. Development  
475 of InGaN-Based Red LED Grown on (0001) Polar Surface. *Appl.*  
476 *Phys. Express* **2014**, *7*, No. 071003.
- (28) Hashimoto, R.; Hwang, J.; Saito, S.; Nunoue, S. High-Efficiency  
477 Yellow Light-Emitting Diodes Grown on Sapphire (0001) Substrates. *478*  
*Phys. Status Solidi C* **2014**, *11*, 628.
- (29) Zhuang, Z.; Iida, D.; Ohkawa, K. InGaN-based red light-  
479 emitting diodes: from traditional to micro-LEDs. *Jpn. J. Appl. Phys.* *480*  
**2022**, *61*, SA0809.
- (30) Li, P.; Li, H.; Zhang, H.; Lynsky, C.; Iza, M.; Speck, J. S.;  
483 Nakamura, S.; DenBaars, S. P. Size-Independent Peak External  
484 Quantum Efficiency (>2%) of InGaN Red Microlight-Emitting  
485 Diodes with An Emission Wavelength over 600 nm. *Appl. Phys.* *486*  
*Lett.* **2021**, *119*, No. 081102.
- (31) Li, P.; Li, H.; Zhang, H.; Yang, Y.; Wong, M. S.; Lynsky, C.; Iza,  
488 M.; Gordon, M. J.; Speck, J. S.; Nakamura, S.; DenBaars, S. P. Red  
489 InGaN micro-light-emitting diodes (>620 nm) with a peak external  
490 quantum efficiency of 4.5% using an epitaxial tunnel junction contact. *491*  
*Appl. Phys. Lett.* **2022**, *120*, 121102.
- (32) Wong, M. S.; Hwang, D.; Alhassan, A. I.; Lee, C.; Ley, R.;  
493 Nakamura, S.; DenBarrs, S. P. High efficiency of III-nitride micro-  
494 light emitting diodes by sidewall passivation using atomic layer  
495 deposition. *Opt. Express* **2018**, *26*, 21324–21331.
- (33) Day, J.; Li, J.; Lie, D. Y. C.; Bradford, C.; Lin, J. Y.; Jiang, H. X.  
497 III-Nitride full-scale high-resolution microdisplays. *Appl. Phys. Lett.* *498*  
**2011**, *99*, No. 031116. *499*